

## THERMO-ECONOMIC SIMULATION OF FOUR POWER GENERATIONS BASED ON GENETIC ALGORITHM

by

**Chao LUO<sup>a,b,c\*</sup>**

<sup>a</sup>School of Architecture and Civil Engineering, Huizhou University, Huizhou, China

<sup>b</sup>Key Laboratory of Efficient Utilization of Low and Medium Grade Energy, Tianjin University, Ministry of Education, Tianjin, China

<sup>c</sup>Guangzhou Institute of Energy Conversion, Chinese Academy of Sciences, Guangzhou, China

Original scientific paper

<https://doi.org/10.2298/TSCI211102027L>

*The thermodynamic and economic suitability of four geothermal power systems is analyzed. When the heat source temperature ranges from 100-150 °C, the performance indicators of power capacity per unit geo-fluid, exergy efficiency, payback period, net present value and internal rate of return for four types of the power system are calculated. The results show that when the heat source temperature increases from 100-150 °C, the power capacity per unit geo-fluid for single flash, organic rankine cycle (ORC), double flash, and flash-ORC system increases from 2.26-7.72 kWh/t, 2.05-8.37 kWh/t, 2.96-9.96 kWh/t, and 2.76-9.82 kWh/t, respectively, and the performance indicators of two-stage energy conversion systems are better than single systems. R245fa is selected as the working fluid based on anti-scaling and better performance. When the heat source temperature is 130 °C, the payback period, net present value and internal rate of return of flash-binary power system are six years, 2508000 US\$ and 16.09%, respectively. The research shows that, unlike the single objective optimization of the two power systems, the multi-objective feasibility analysis is a technical integration innovation of the existing research. The research can provide technical support for power construction and realize the sustainable development of clean energy in China.*

**Key words:** *geothermal power generation, flash; binary, flash-binary, numerical simulation, exergy*

### Introduction

Energy is an important material basis for the survival and development of human society. With the adjustment of international energy strategy, the fourth industrial revolution represented by green sustainable development has come. The energy system will develop in a clean, efficient, and safe direction. Green energy and a low-carbon economy have become research hotspots in countries [1, 2]. Increasing the proportion of renewable energy in the energy systems of countries and developing renewable clean energy are the fundamental ways to reduce GHG emissions and solve the global climate change problem. Geothermal resources have the characteristics of abundant reserves and wide distribution. Geothermal energy is

---

\* Author's e-mail: luochao@hzu.edu.cn

renewable energy with low carbon, environmental protection and good stability, which plays a vital role in China's carbon neutrality goal by 2060.

Global installed geothermal power plant capacity in 2020 is 15950 MW, an increase of about 30% compared to 2015. The top five countries of power capacity are the USA, Indonesia, the Philippines, Turkey, and Kenya. The total installed capacity is only 34.8 MW in China [3]. Most research on geothermal power stations in the world focuses on high temperature resources with a temperature higher than 150 °C. Geothermal power generation has the characteristics of high utilization factor of installed capacity. Some scholars have done research on thermal and economic optimization design of the system. The flash-binary power system has the highest thermo-electric conversion efficiency and the lowest construction cost of the power station compared with single and double flash system [4]. Franco [5] proposed a new optimized objective of hot water consumption per unit power capacity for hydrothermal geothermal resources with temperatures ranging from 110 to 160 °C. Hardi *et al.* [6] analysed the energy and exergy of the Dieng geothermal power station with the high temperature in Indonesia. According to the measured data, he pointed out that the steam turbine should be mainly repaired. Gnaifaid and Ozcan [7] provides a composite geothermal system consisting of flash-binary power generation, refrigeration, heat supply, and seawater desalination device. The exergy efficiency of the system is about 58%, but economic indicators are not analyzed in the paper. Hu *et al.* [8] proposed the geothermal-solar combined power generation system, which solved the problem affected by the surrounding environment. The paper has given the net present value of the system, but lacked the analysis of the internal rate of return. Jalili *et al.* [9] only analysed the environmental and economic efficiency of the flash-binary power system by using the emergy concept, and pointed out that the economic emergy rate and ecological emergy rate are 34.1% and 4.0%, respectively. Yousefi *et al.* [10] built four models of single flash, double flash, single flash-cascade utilization, and double flash-cascade utilization, and pointed out that the two models after cascade utilization can save 2374000 and 636000 US\$, respectively. Wang *et al.* [11, 12] studied the combined system of ORC and floor radiant heating, the results show that the thermal and exergy efficiency of the combined system are 19.2% and 53.3%, respectively. DiPippo [13] gives the applications, case studies and environmental impact for geothermal power plants. Cetin and Kecebas [14] compared the influence of different algorithms on the thermal performance of the actual geothermal power plant, and adopted the annealing simulation algorithm to optimize the system with better results, which can achieve greater power generation capacity and less non-condensable gas. In this study, in order to optimize the performance of such a system using the simulated genetic algorithm [14].

In China, the temperature of most geothermal resources is lower than 150 °C. Therefore, thermal analysis and economic analysis must be carried out on the medium-high temperature geothermal resources with temperature between 100 °C and 150 °C. These targeted studies will provide technical and methodological support for power station construction in Tibet, western Sichuan, and Yunnan, and will increase the proportion of renewable energy in power generation in China.

## **Modeling of geothermal power generation system**

### *Physical models of four systems*

At present, the commercial geothermal power generation systems include single flash, double flash, and ORC. The combined power system will improve the resource utiliza-

tion efficiency of high temperature geothermal resources. The combined power system is any combination of the previous three power systems. The combined power system mainly includes flash-binary or binary-flash system. Figure 1 gives the four schematic diagrams of the power systems:

- *Single flash geothermal power system.* As shown in fig. 1(a), the geo-fluid from a production well first flows into a throttle valve, and then enters the separator. The steam from the separator was used to promote the turbine, at the same time, the saturated water from the separator is pumped to the rejection well. The advantages of the single flash system are simple structure, less investment and a short payback period. The disadvantages are complicated site installation and construction, and easy to scale and corrode.
- *Double flash geothermal power system.* As shown in fig. 1(b), the geo-fluid from the production well is sent to the high pressure separator through the high pressure throttle valve first, and then the high pressure steam enters a high pressure turbine. At the same time, the high temperature saturated water from the high pressure separator enters to low pressure separator through the low pressure throttle valve. The low pressure steam enters a low pressure turbine, and then the low temperature saturated water is pumped into the rejection well. At last, the high pressure and low pressure steam flow into condenser after expansion. The advantage of the double flash system is that the thermal efficiency is higher than other systems, and the disadvantage is that the site installation and construction are complicated, and the debugging is difficult. As a result, the double flash system is more suitable for the occasion when the heat sources temperature is above 140 °C.
- *The ORC.* As shown in fig. 1(c), the geo-fluid from a production well first flows into the vaporizer, and then enters preheater, and finally is pumped to rejection well. The working fluid is vaporized in the vaporizer and then enters the turbine to generate electricity. Steam discharged from the turbine is condensed by cooling water in the condenser. The ORC with a regenerative device will effectively improve the efficiency of the power generation system. The advantage of the ORC is that the system is applied widely and is easy to install. The disadvantage is that the working fluid is of high price and has a risk of leakage.
- *Flash-binary geothermal power system.* As shown in fig. 1(d), the flash-binary power system consists of a sub-flash system and a sub-binary cycle. Geo-fluid flows into a separator after being decompressed by a throttle valve, and the steam from the separator was used to promote the turbine in a sub-flash system. At the same time, the saturated water from the separator is used as heat source for sub-binary cycle. The saturated water enters the vaporizer, preheater in turn, and then flows into the rejection well. The organic working fluid is pumped into the preheater from the condenser and then into the vaporizer. The superheated vapor flows into another turbine, and then is exhausted to the condenser. The advantage of the flash-binary system is that resource utilization efficiency is improved, and energy waste is reduced. The disadvantage is that the site installation and construction are complicated. The flash-binary system is more suitable for heat sources above 130 °C.

The temperature-entropy,  $T$ - $s$ , diagrams of four systems are shown in fig. 2. Dashed lines 3-4s and 9-10s represent the ideal isentropic expansion process in the turbine, respectively. The actual expansion process of the turbine is 3-4 and 9-10, respectively. The exhaust steam after expansion of the steam turbine is condensed by the condenser and then discharged from the flash system. The exhaust steam of the high pressure and low pressure turbine is mixed at the state Point 5 for the double system, and then flows into the condenser.

Dashed lines 6-7s represent the ideal isentropic expansion process in the turbine for ORC. The actual expansion process of the turbine is 6-7. Curves 11-12 and 5-6 represent the

actual expansion process of the gas in the sub-flash system and sub-binary cycle, respectively, while curves 11-12s and 5-6s represent the ideal expansion process of the gas in the sub-flash system and sub-binary cycle, respectively.

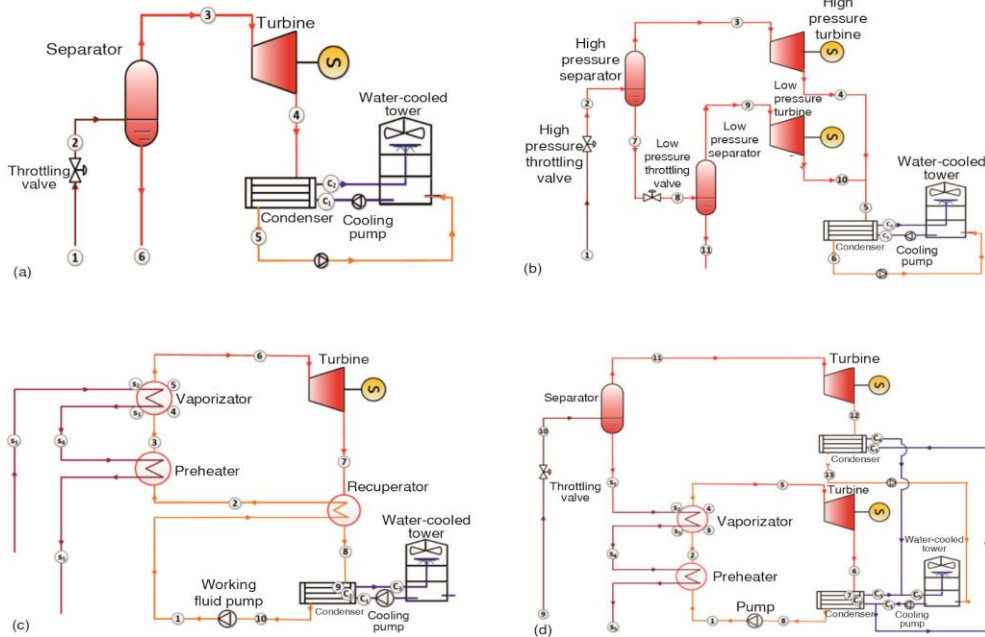


**Figure 1.** Schematic diagram for four power systems; (a) single flash, (b) double flash, (c) ORC, and (d) flash-binary

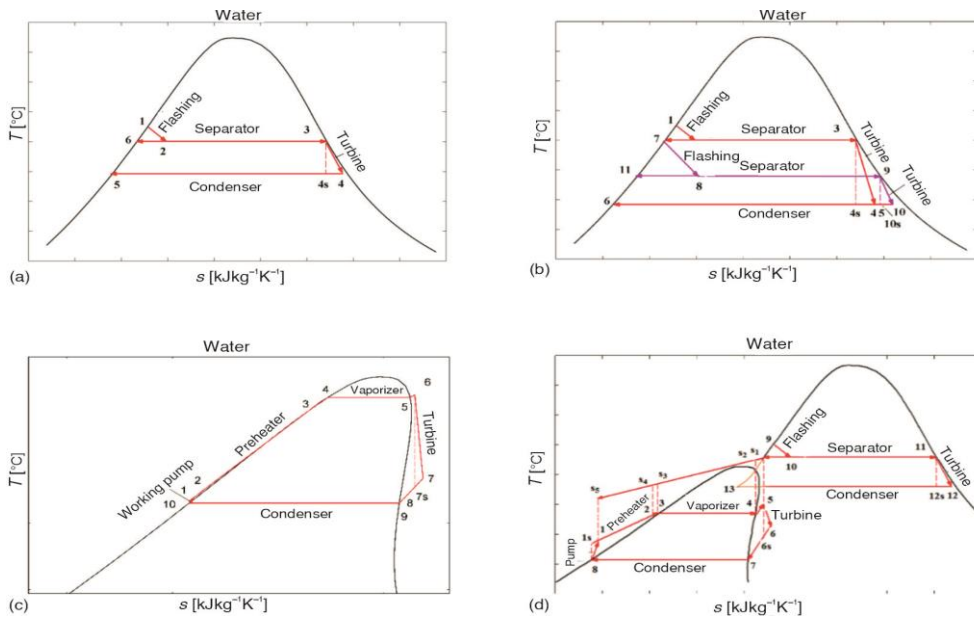


**Figure 2.** The  $T$ - $s$  diagram for four power systems; (a) single flash, (b) double flash, (c) ORC, and (d) flash-binary

### Mathematical model

The mass and energy balance of the system and equipment:

$$\dot{m}_{in} = \sum \dot{m}_{out} \quad (1)$$

$$Q_{in} = W + \sum Q_{out} \quad (2)$$

where  $\dot{m}_{in}$  [ $\text{kgs}^{-1}$ ] is the mass-flow rate of inlet geo-fluid,  $\dot{m}_{out}$  [ $\text{kgs}^{-1}$ ] – the mass-flow rate of outlet geo-fluid,  $Q_{in}$  [ $\text{kJ s}^{-1}$ ] – the heat input energy,  $W$  [ $\text{kJ s}^{-1}$ ] – the output useful work of the system, and  $Q_{out}$  [ $\text{kJ s}^{-1}$ ] – the output heat energy.

The thermodynamic performance indexes of thermal efficiency,  $\eta_1$ , exergy efficiency,  $\eta_2$ , power output per unit geo-fluid,  $Ne$ , payback period,  $\tau_{PB}$ , net present value,  $NPV$ , and internal rate of return,  $IRR$ , can be expressed as:

$$\eta_1 = \frac{W_{net}}{\Delta Q} \quad (3)$$

$$\eta_2 = \frac{W_{net}}{E_{in}} \quad (4)$$

$$Ne = \frac{W_{net}}{3.6\dot{m}_{in}} \quad (5)$$

$$\tau_{PB} = \frac{TCC}{ANCF} \quad (6)$$

$$NPV = \sum_{\tau=0}^{Ny} \left[ Y_{\tau} \frac{1}{(1+i_{eff})^{\tau}} \right] \quad (7)$$

$$NPV = \sum_{\tau=0}^{Ny} \left[ Y_{\tau} \frac{1}{(1+IRR)^{\tau}} \right] = 0 \quad (8)$$

where  $W_{net}$  [kW] is the net power output of the system,  $\Delta Q$  [kW] – the circulating heating energy of geothermal fluid,  $E_{in}$  [kW] – the exergy rate of geothermal fluid,  $TCC$  [US\$] – the total capital cost,  $ANCF$  [US\$ per year] – the average annual net cash inflow,  $Y_{\tau}$  [US\$] – the net cash inflow at the end of the year,  $Ny$  – the life cycle of the power station (25 years), and  $i_{eff}$  – the effective interest rate of the project (8%). When the net present value,  $NPV$ , is 0, the effective interest rate,  $i_{eff}$ , is the internal rate of return, which is generally calculated by computer iteration.

Equations (1)-(5) are used for the thermodynamic analysis. The properties of water and organic working fluid are assumed by the software of REFPROP 9.0. In *Appendix*, tabs.1-3 are given the balance equations of related equipment for four power generation systems, the purchased equipment cost (PEC) and total capital cost (TCC), respectively. The PEC of the single flash, double flash, ORC, and flash-binary are 299717 US\$, 399491 US\$, 283649 US\$, and 312137 US\$, respectively. The TCC of the single flash, double flash, ORC, and flash-binary are 3267609 US\$, 3513147 US\$, 3228059 US\$, and 3298169 US\$ [15-17].

### Results of thermodynamic simulation

Figure 3 shows the effect of flash temperature on  $Ne$  and  $\eta_2$  for the single flash power system when the geo-fluid temperature ranges from 80-150 °C. When the geo-fluid tem-

perature is constant, the  $Ne$  and  $\eta_2$  increase first and then decrease with increasing flash temperature. When the geo-fluid temperatures are 100 °C, 130 °C, and 150 °C, the maximum  $Ne$  are 2.26 kWh/t, 5.16 kWh/t, and 7.72 kWh/t, respectively, the maximum  $\eta_2$  are 18.37%, 24.07%, and 26.91%, respectively, the optimum flash temperatures are 71 °C, 84 °C, and 94 °C, respectively. The  $Ne$  is positively correlated with the  $\eta_2$ , and the maximum  $Ne$  and  $\eta_2$  increase with increasing geo-fluid temperature.

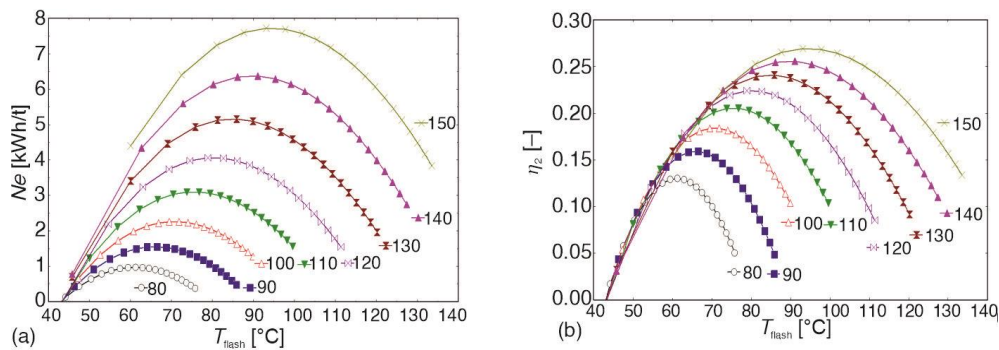


Figure 3. The influence of  $T_{\text{flash}}$  on  $Ne$  and  $\eta_2$  for single flash system; (a)  $Ne$  and (b)  $\eta_2$

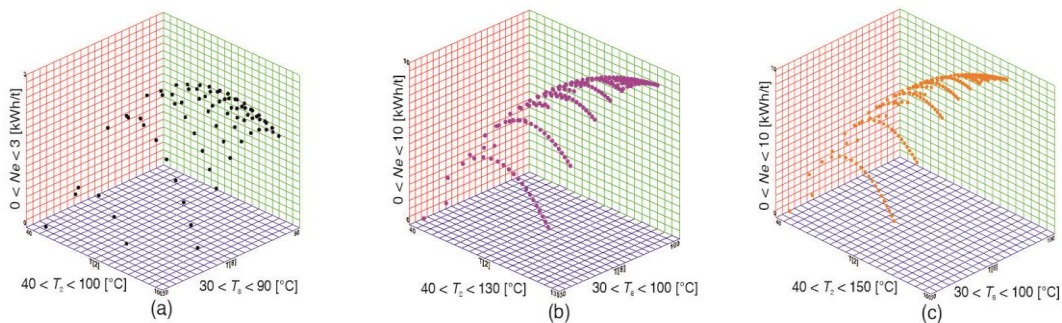


Figure 4. The relationship between  $Ne$  and separator temperature; (a)  $T_{\text{source}} = 100$  °C, (b)  $T_{\text{source}} = 130$  °C, and (c)  $T_{\text{source}} = 150$  °C

Figure 4 shows the effect of high pressure separator temperature,  $T_2$ , and low pressure separator temperature,  $T_8$ , on  $Ne$  for the double flash power system when the geo-fluid temperatures are 100 °C, 130 °C, and 150 °C, respectively. When the  $T_2$  is constant, the  $Ne$  creases first and then decreases with increasing  $T_8$ . Similarly, when the  $T_8$  is constant, the  $Ne$  creases first and then decreases with increasing  $T_2$ . The simulation results show that when the geo-fluid temperatures are 100 °C, 130 °C, and 150 °C, the maximum  $Ne$  are 2.96 kWh/t, 6.70 kWh/t, and 9.96 kWh/t, respectively, the maximum  $\eta_2$  are 24.08%, 31.25%, and 34.72%, respectively, the optimum high pressure separator temperature  $T_2$  is 77 °C, 100 °C, and 109 °C, respectively, the optimum low pressure separator temperature  $T_8$  is 55 °C, 71 °C, and 70 °C, respectively. When the geo-fluid temperature is 130 °C, the high pressure separator is in a positive pressure state, which will greatly reduce the volume of the separator and reduce the cost of equipment.

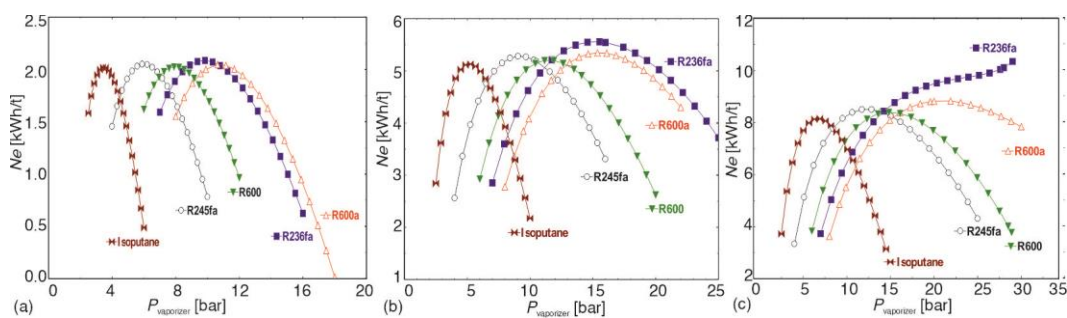
The selection of working fluid has an important influence on the performance of ORC. Dry organic working fluid is usually selected as the alternative working fluid for the ORC, which can prevent the larger superheat of the inlet expander gas and the exhaust gas of

the expander from entering the two-phase zone. The slope  $dT/ds$  of the saturated steam line for the dry organic working fluid is greater than 0. The performance of ORC with five working fluids is compared, and then one of the five working fluids is selected in the ORC. The five alternative working fluids are R236fa, R600a, R600, R245fa, and Isoputane. The physical parameters of the five working fluids (REFPROP 9.0) are shown in tab. 1.

**Table 1. The parameters of working fluids**

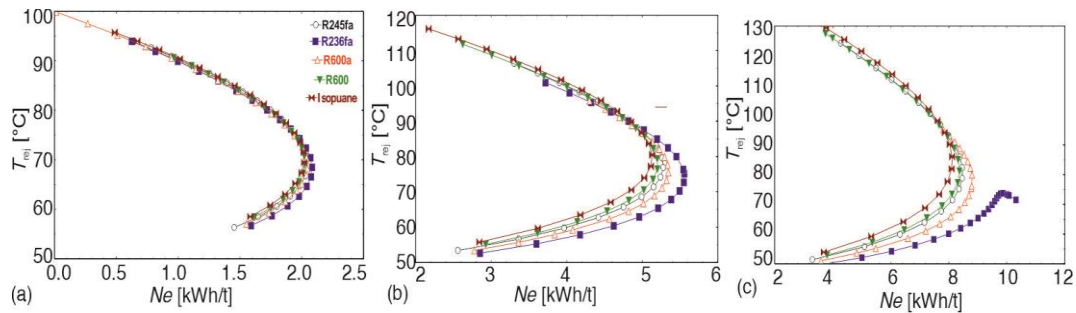
Alternative working fluids	Critical temperature [°C]	Critical pressure [bar]	Boiling point [°C]	Ozone depression potential	Global warming potential
R236fa	124.92	32.00	-1.44	0	6300
R600a	134.66	36.29	-11.75	0	20
R600	151.01	37.97	-0.49	0	20
R245fa	154.00	36.51	15.10	0	820
Isoputane	187.20	33.70	30.00	0	

Figure 5 shows the effect of vaporizer pressure on  $Ne$  for ORC when geo-fluid temperatures are 100 °C, 130 °C, and 150 °C, respectively. The  $Ne$  increases first and then decreases with increasing vaporizer pressure when the geo-fluid temperatures are 100 °C and 130 °C. However, the  $Ne$  increases with increasing vaporizer pressure for R236fa when the geo-fluid temperature is 150 °C because the working fluid is in a transcritical state. The higher geo-fluid temperature is, the greater maximum  $Ne$  for the same working fluid. When arranged according to the maximum  $Ne$  available, these working fluids are R236fa, R600a, R245fa, Isoputane, and R600 by descending. When the temperature of the geo-fluid is higher, the vaporizer pressure of the first three working fluids is higher than the last two, which means these working fluids will require higher pressure containers.



**Figure 5. The effect of vaporizer pressure on  $Ne$  for ORC; (a)  $T_{source} = 100$  °C, (b)  $T_{source} = 130$  °C, and (c)  $T_{source} = 150$  °C**

Figure 6 shows the change effect of  $Ne$  on geo-fluid rejection temperature,  $T_{rej}$ , of five working fluids. To prevent the scaling of equipment, the  $T_{rej}$  is usually limited to about 70 °C. When  $T_{rej}$  is higher than 70 °C, the  $Ne$  of R236fa and R600a is greater than that of the other three working fluids. However, when the local fluid temperature is relatively high, it is easy to form a supercritical cycle, leading to the decomposition of the working fluid and low exergy efficiency. The larger  $T_{rej}$  is, the higher  $Ne$  of R245fa is than that of the R600 and Isoputane. The ORC with R245fa working fluid is of large  $Ne$  and high  $\eta_2$ , while the vaporizer pressure is not too high, and there is a higher rejection geo-fluid temperature to prevent scaling. The R245fa is selected for the ORC. The vaporizer pressure of ORC is between 5-15 bar,  $Ne$  is between 2.05-8.48 kWh/t,  $\eta_1$  is between 5.7-10.4%, and  $\eta_2$  is between 16.5-29.4%, respectively, when the rejection geo-fluid temperature is above 70 °C.



**Figure 6.** The effect of  $Ne$  on geo-fluid rejection temperature  $T_{rej}$  for ORC; (a)  $T_{source} = 100\text{ }^{\circ}\text{C}$ , (b)  $T_{source} = 130\text{ }^{\circ}\text{C}$ , and (c)  $T_{source} = 150\text{ }^{\circ}\text{C}$  (for color image see journal web site)

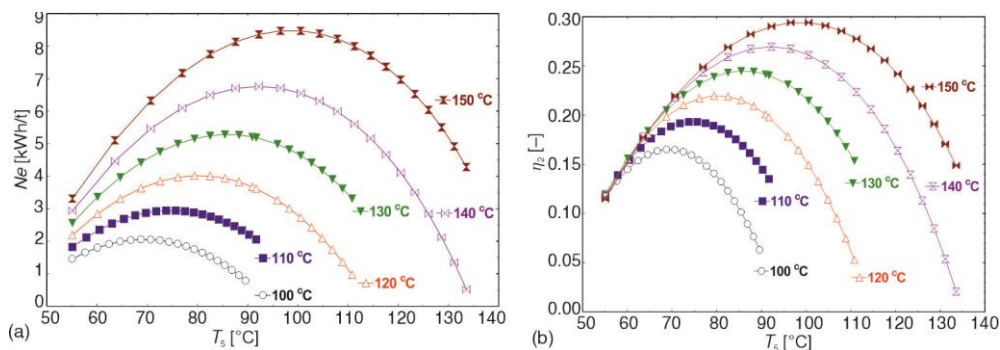


**Figure 7.** The effect of vaporizer temperature  $T_5$  on  $Ne$  and  $\eta_2$  for ORC; (a)  $Ne$  and (b)  $\eta_2$

Figure 7 shows the effect of vaporizer temperature  $T_5$  on  $Ne$  and  $\eta_2$  of the ORC. When the geo-fluid temperature is constant, the  $Ne$  and  $\eta_2$  increase first and then decrease with increasing  $T_5$ . There is an optimal vaporizer temperature to maximize the  $Ne$  and  $\eta_2$  under different geo-fluid temperatures. The optimal vaporizer temperature increases approximately linearly with the increase of geo-fluid temperature. When the geo-fluid is  $130\text{ }^{\circ}\text{C}$ , the maximum  $Ne$  and  $\eta_2$  are  $5.21\text{ kWh/t}$  and  $24.14\%$ , respectively, the optimal vaporizer temperature and pressure are  $86\text{ }^{\circ}\text{C}$  and  $9.18\text{ bar}$ , respectively. The higher geo-fluid temperature is, the greater maximum  $Ne$  and  $\eta_2$  are.

Figure 8 shows the influence of separator pressure,  $P_{separator}$ , and vaporizer pressure,  $P_{vaporizer}$ , on  $Ne$  for flash-binary power system when the geo-fluid temperature are  $100\text{ }^{\circ}\text{C}$ ,  $130\text{ }^{\circ}\text{C}$ , and  $150\text{ }^{\circ}\text{C}$ , respectively. When the  $P_{separator}$  is constant, the  $Ne$  increases first and then decreases with increasing  $P_{vaporizer}$ . When the  $P_{vaporizer}$  is constant, the  $Ne$  increases first and then decreases with increasing  $P_{separator}$ . Therefore, there is a couple of optimal value, which makes  $Ne$  reach the maximum under different geo-fluid temperatures. The  $Ne$  will increase with increasing geo-fluid temperatures. When the geo-fluid temperature is  $100\text{ }^{\circ}\text{C}$ , the  $Ne$  and  $\eta_2$  are  $2.76\text{ kWh/t}$  and  $22.60\%$ , respectively, and the corresponding separator and vaporizer temperature are  $79\text{ }^{\circ}\text{C}$  and  $61\text{ }^{\circ}\text{C}$ , respectively. When the geo-fluid temperature is  $130\text{ }^{\circ}\text{C}$ , the  $Ne$  and  $\eta_2$  are  $6.48\text{ kWh/t}$  and  $30.53\%$ , respectively, and the corresponding separator and vaporizer temperature are  $100\text{ }^{\circ}\text{C}$  and  $71\text{ }^{\circ}\text{C}$ , respectively. When the geo-fluid temperature is  $150\text{ }^{\circ}\text{C}$ , the  $Ne$  and  $\eta_2$  are  $9.92\text{ kWh/t}$  and  $34.63\%$ , respectively, and the corresponding separator and vaporizer temperature are  $115\text{ }^{\circ}\text{C}$  and  $80\text{ }^{\circ}\text{C}$ , respectively. The separator pressure is greater than 1 atmosphere when the geo-fluid is higher  $130\text{ }^{\circ}\text{C}$ , which will result in the reduction of the volume and cost of the separator.

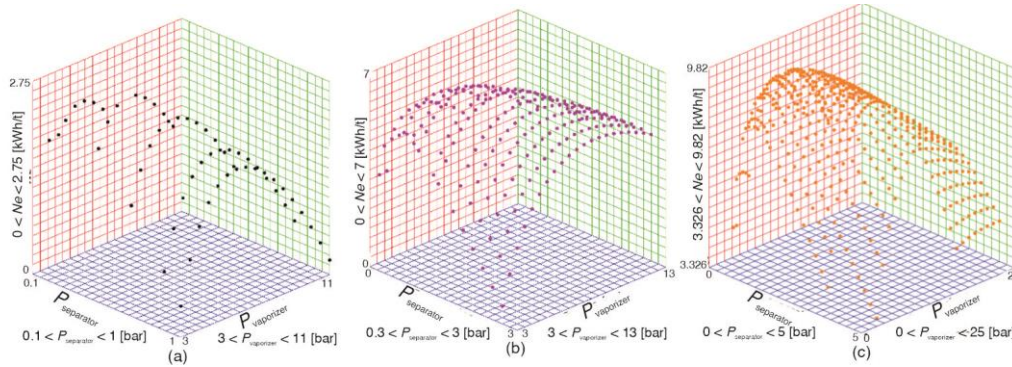


**Figure 8.** The influence of separator and vaporizer pressure on  $Ne$  for flash-binary system; (a)  $T_{source} = 100\text{ }^{\circ}\text{C}$ , (b)  $T_{source} = 130\text{ }^{\circ}\text{C}$ , and (c)  $T_{source} = 150\text{ }^{\circ}\text{C}$

Table 2 shows the thermodynamic performance comparison of four power systems when the cooling temperature is  $25\text{ }^{\circ}\text{C}$ . The thermal performance of the double flash and flash-binary power system is better than that of the single flash and ORC power system. With the increase of geo-fluid temperature, the thermodynamic performance of ORC is gradually better than that of single flash system, and the thermodynamic performance of flash-binary system is gradually close to that of double flash system. When the geo-fluid temperature is  $130\text{ }^{\circ}\text{C}$ , the power output per unit geo-fluid of ORC is higher than that of single flash system. The higher the geo-fluid temperature is, the better thermal performance of ORC is.

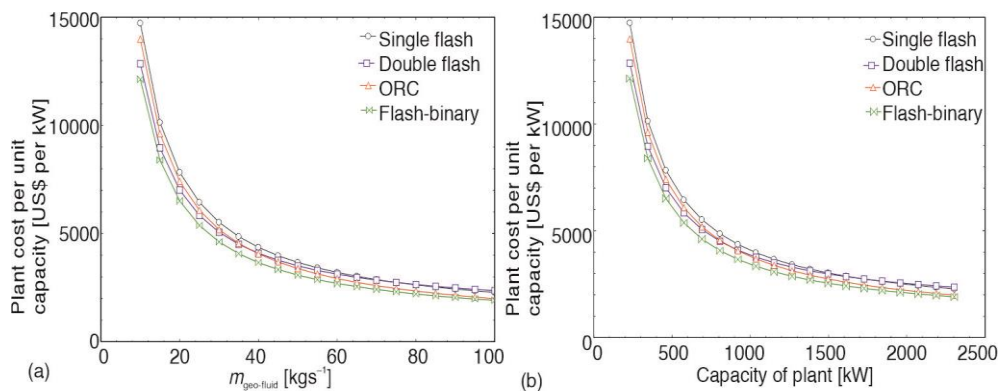
**Table 2.** The thermodynamic performance comparison for power systems

Geo-fluid temperature [°C]	$Ne$ [kWh/t]				$\eta_2$ [%]				$T_{rej}$ [°C]			
	Single flash	ORC	Double flash	Flash-binary	Single flash	ORC	Double flash	Flash-binary	Single flash	ORC	Double flash	Flash-binary
100	2.26	2.05	2.96	2.76	18.37	16.51	24.08	22.6	70.74	69.31	62.24	62.46
110	3.10	2.94	4.05	3.83	20.52	19.33	26.82	25.56	75.5	72.40	64.68	65.28
120	4.07	4.02	5.29	5.07	22.40	21.97	29.18	28.18	80.23	75.11	67.51	67.99
130	5.16	5.21	6.70	6.48	24.07	24.14	31.25	30.53	84.05	77.81	70.56	70.63
140	6.38	6.76	8.25	8.06	25.55	26.95	33.08	32.66	89.65	79.25	73.69	73.11
150	7.72	8.37	9.96	9.82	26.91	29.44	34.72	34.63	94.35	81.31	76.68	75.49

### Results of economic simulation

Figure 9 show the influence of geo-fluid mass-flow rate and plant installed capacity on plant cost per unit capacity for the four power systems. The plant cost per unit capacity gradually decreases with increasing the geo-fluid mass-flow rate and plant installed capacity. When the geo-fluid mass-flow rate and plant installed capacity are less than  $36\text{ kg/s}$  and  $700\text{ kW}$ , respectively, the plant cost per unit capacity in descending order is single flash, ORC, double flash, and flash-binary power system, and it is approximately over  $4500\text{ US\$}$  per kW. When the geo-fluid mass-flow rate is greater than  $36\text{ kg/s}$  and less than  $75\text{ kg/s}$ , and the plant installed capacity is greater than  $700\text{ kW}$  and less than  $1500\text{ kW}$ , the plant cost per unit capacity in descending order is single flash, double flash, ORC, and flash-binary power system, and

it is approximately over 2500-4500 US\$ per kW. When the geo-fluid mass-flow rate and plant installed capacity are greater than 75 kg/s and 1500 kW, respectively, the plant cost per unit capacity in descending order is double flash, single flash, ORC, and flash-binary power system, and it is approximately under 2500 US\$ per kW. When the plant installed capacity is greater than 1500 kW, the sensitivity of mass-flow rate and installed capacity on plant cost per unit capacity decreases. When the geo-fluid mass-flow rate is 150 tone per hours (42 kg/s), the plant installed capacity of single flash, double flash, ORC and flash-binary power systems is 773.7, 1004.0, 822.5, and 981.0 kW, respectively, and the corresponding plant cost per unit capacity are 4106, 3876, 3812, and 3446 US\$ per kW, respectively.



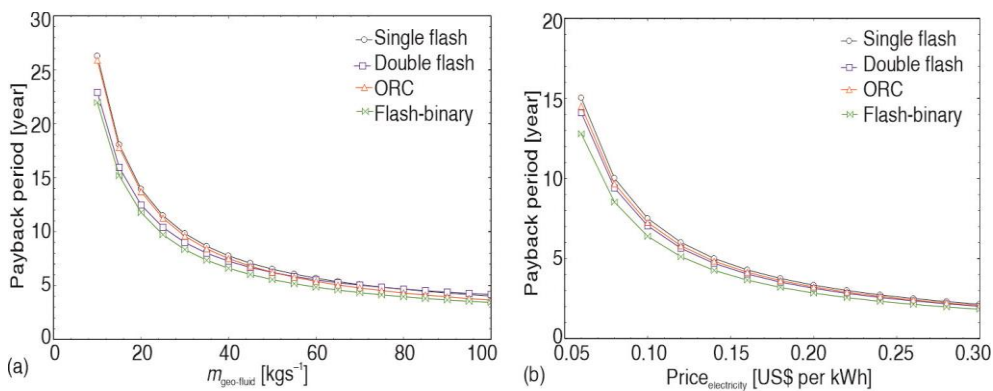
**Figure 9. The influence of geo-fluid mass rate and plant capacity on plant cost per unit capacity; (a) geo-fluid mass-flow rate and (b) plant capacity**

Figure 10 shows the influence of geo-fluid mass-flow rate and electricity price on the payback period for the four power systems. The payback period gradually decreases with increasing the geo-fluid mass-flow rate because of increasing available electric energy. The payback period of double flash system is gradually longer than that of ORC and single flash system with increasing geo-fluid mass-flow rate. The payback period of flash-binary system is the shortest of the four systems under the same conditions. When the geo-fluid mass-flow rate is less than 45 kg/s, the payback period in descending order is single flash, ORC, double flash, and flash-binary power system, and the payback period is approximately over 6.5 years. When the geo-fluid mass-flow rate is more than 45 kg/s and less than 75 kg/s, the payback period in descending order is single flash, double flash, ORC, and flash-binary power system, and the payback period is between 4.5 and 6.5 years. When the geo-fluid mass-flow rate is more than 75 kg/s, the payback period in descending order is double flash, single flash, ORC and flash-binary power system, and the payback period is approximately under 4.5 years.

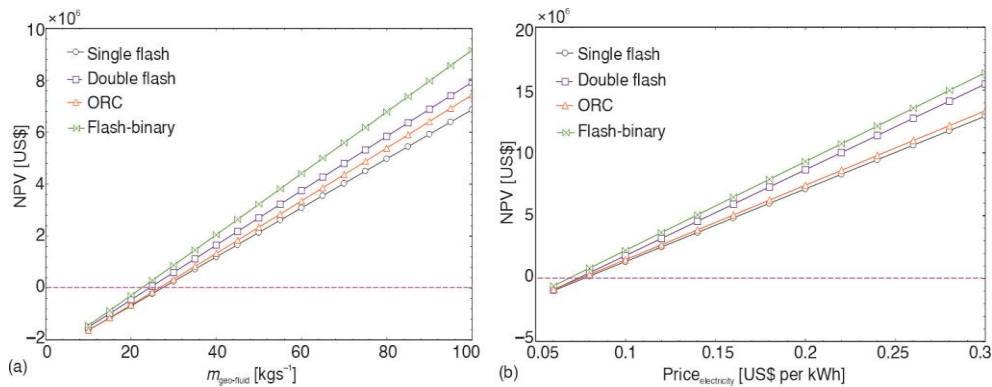
The payback period gradually decreases with increasing the electricity price because of increasing available revenue. When the electricity price increases from 0.06 to 0.20 US\$ per kWh, the payback period for single flash, ORC, double flash, and flash-binary systems are reduced from 15.0-3.3 years, 14.5-3.2 years, 14.0-3.1 years, and 12.8-2.8 years, respectively. When the electricity price is higher than 0.20 US\$ per kWh, the payback period of the power systems changes a little with increasing the electricity price, which is maintained at about 2-3 years.

Figure 11 shows the influence of geo-fluid mass-flow rate and electricity price on NPV for the four power systems. The NPV gradually increases with increasing the geo-fluid mass-flow rate because of increasing available electric energy. The NPV of the four systems

in descending order is single flash-binary, double flash, ORC, and flash power system. When the NPV is 0, the geo-fluid mass-flow rate of flash-binary, double flash, ORC, and single flash system are 21.3 kg/s, 21.4 kg/s, 26.6 kg/s, and 27.3 kg/s, respectively. It is necessary to make NPV bigger than zero for power station economic. The NPV gradually increases with increasing the electricity price because of increasing available revenue. The NPV of the flash-binary power system is the largest and the single flash system is the smallest with the same electricity price. When the NPV is 0, the electricity prices of flash-binary, double flash, ORC, and single flash systems are 0.06552, 0.06693, 0.07469 and 0.07664 US\$ per kWh, respectively.



**Figure 10. The influence of geo-fluid mass-flow rate and electricity price on payback period; (a) geo-fluid mass-flow rate and (b) electricity price**



**Figure 11. The influence of geo-fluid mass-flow rate and electricity price on NPV; (a) geo-fluid mass-flow rate and (b) electricity price**

Figure 12 shows the influence of geo-fluid mass-flow rate and electricity price on IRR for the four power systems. The IRR gradually increases with increasing the geo-fluid mass-flow rate. The sensitivity of mass-flow rate on IRR for the flash-binary system is greater than that for the other three power systems. The revenue of the flash-binary power system is the largest of the four systems under the same mass-flow rate condition. The NPV gradually increases with increasing the electricity price. The IRR of the flash-binary power system is the largest and the single flash system is the smallest under the same electricity price. When the IRR is 8%, the electricity prices of flash-binary, double flash, ORC, and single flash systems are 0.06552, 0.06693, 0.07469, and 0.07664 US\$ per kWh, respectively.

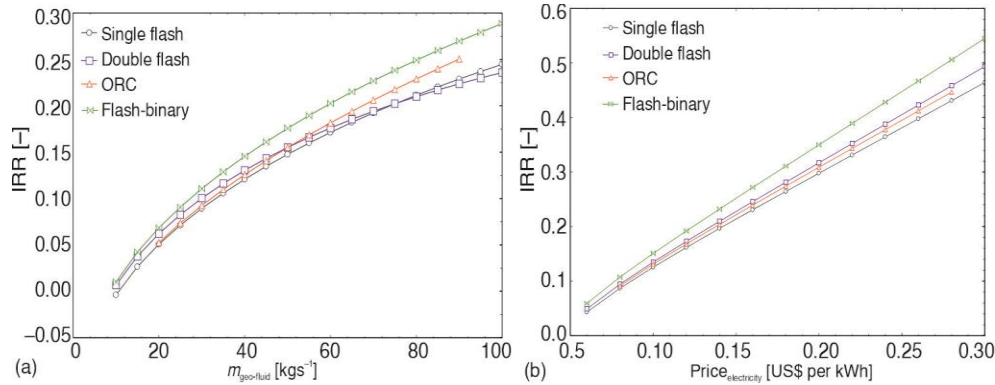


**Figure 12. The influence of geo-fluid mass-flow rate and electricity price on IRR; (a) geo-fluid mass-flow rate and (b) electricity price**

Table 3 shows the economic comparison for the four power systems. The economic performance of flash-binary is the best, and the economic performance of double flash, ORC, and single flash systems decrease in turn. Based on the economic data analysis, a flash-binary power system is more suitable for geothermal resources when the temperature is above 130 °C.

**Table 3. The economic comparison for four power systems**

Power systems	Payback period [Years]	NPV [US\$]	IRR [%]
Single flash	7.508	1352000	12.55
Double flash	6.211	2485000	15.56
ORC	7.248	1501000	13.09
Flash-binary	6.031	2508000	16.09

## Conclusions

Four power systems are comprehensively compared and analyzed for mid-high geothermal resources based on thermodynamics and economics. The conclusions are as follows.

- The performance of ORC is better than single flash with increasing geo-fluid temperature, and the performance of flash-binary system is gradually close to that of double flash system with increasing geo-fluid temperature. When the geo-fluid temperature is 130 °C, the  $N_e$  of flash-binary, double flash, ORC, and single flash are 6.481 kWh/t, 6.695 kWh/t, 5.205 kWh/t, and 5.160 kWh/t, respectively. It is better to apply the flash-binary power system when the geo-fluid temperature is higher than 130 °C.
- The higher geo-fluid temperature is, the better performance of ORC is. The ORC with R245fa working fluid is of large  $N_e$  and high  $\eta_2$ , while the vaporizer pressure is not too high, and there is a higher rejection geo-fluid temperature to prevent scaling. The R245fa is preferred as the working fluid for ORC.
- The plant cost per unit capacity gradually decreases with the increase of the geo-fluid mass-flow rate and plant installed capacity. When the geo-fluid mass-flow rate is 150 t per hours, the plant cost per unit capacity of single flash, double flash, ORC, and flash-binary power systems are 4106, 3876, 3812, and 3446 US\$ per kW, respectively, and the corresponding payback periods are 7.5, 6.2, 7.2, and 6.0 years, respectively.
- The higher electricity price is, the better economy of power system is. When the electricity prices of flash-binary, double flash, ORC, and single flash systems are higher than

0.06552, 0.06693, 0.07469, and 0.07664 US\$ per kWh, respectively, the corresponding NPV and IRR are higher than 0 US\$ and 8%.

### Acknowledgment

This work is supported by the Science and Technology Planning Project of Huizhou, Guangdong province (2020SD0401029), University Characteristic Innovation Project of Department of Education of Guangdong Province (2020KTSCX143), Indigenous Innovation's Capability Development Program of Huizhou University (HZU202002).

### References

- [1] Hou, P., *et al.*, Effect of Thermal Cycling on Mechanical Properties and Energy Evolution of Sandstone, *Thermal Science*, 24 (2020), 6, pp. 4001-4009
- [2] Denda, S. L., *et al.*, Utilization of Geothermal Springs as a Renewable Energy Source Vranjska Banja Case Study, *Thermal Science*, 23 (2019), 6, pp. 4083-4093
- [3] Hutterer, G. W., Geothermal Power Generation in the World 2015-2020 Update Report, *Proceedings*, World Geothermal Congress, Reykjavik, Iceland. 2020
- [4] Coskun, A., *et al.* Thermodynamic and Economic Analysis and Optimization of Power Cycles for a Medium Temperature Geothermal Resource, *Energy Conversion and Management*, 78 (2014), Feb., pp. 39-49
- [5] Alessandro, F., Marco, V., Optimal Design of Binary Cycle Power Plants for Water-Dominated, Medium-Temperature Geothermal Fields, *Geothermics*, 38 (2009), 4, pp. 379-391
- [6] Hardi, A., *et al.*, Energy and Exergy Analysis of Dieng Geothermal Power Plant, *International Journal of Technology*, 12 (2021), 1, pp. 175-185
- [7] Gnaifaid, H., Ozcan, H., Development and Multiobjective Optimization of an Integrated Flash-Binary Geothermal Power Plant with Reverse Osmosis Desalination and Absorption Refrigeration for Multi-generation, *Geothermics*, 89 (2021), Jan., pp. 1-12
- [8] Hu, S., *et al.*, Thermo-Economic Optimization of the Hybrid Geothermal-Solar Power System: A Data-Driven Method based on Lifetime Off-Design Operation, *Energy Conversion and Management*, 229 (2021), Feb., pp. 1-17
- [9] Jalili, M., *et al.*, Economic and Environmental Assessment using Energy of a Geothermal Power Plant, *Energy Conversion and Management*, 228 (2021), Jan., pp. 1-12
- [10] Yousefi, H., *et al.*, Cascading uses of Geothermal Energy for a Sustainable Energy Supply for Meshkinshahr City, Northwest, Iran, *Geothermics*, 79 (2019), May, pp. 152-163
- [11] Wang, W., *et al.*, Exergoeconomic and Exergoenvironmental Analysis of a Combined Heating and Power System Driven by Geothermal Source, *Energy Conversion and Management*, 211 (2020), May, pp. 1-13
- [12] Wang, Y., *et al.*, Innovative Geothermal-Based Power and Cooling Cogeneration System, Thermodynamic Analysis and Optimization, *Sustainable Energy Technologies and Assessments*, 44 (2021), Apr., pp. 1-19.
- [13] DiPippo, R., *Geothermal Power Plants: Principles, Applications, Case Studies and Environmental Impact*, 2<sup>nd</sup> ed., Butterworth-Heinemann, Elsevier, UK, 2008
- [14] Cetin, G., Kecebas, A., Optimization of Thermodynamic Performance with Simulated Annealing Algorithm: A Geothermal Power Plant, *Renewable Energy*, 172 (2021), July, pp. 968-982
- [15] Bejan, A., *et al.*, *Thermal Design and Optimization*, John Wiley & Sons, Inc., New York, USA, 1996
- [16] Ilas, A., *et al.*, Renewable Power Generation Costs in 2017, International Renewable Energy Agency, Abu Dhabi, United Arab Emirates, pp. 1-12.
- [17] Jon, G. Harold., *et al.*, Renewable Power Generation Costs in 2018, International Renewable Energy Agency, Abu Dhabi, United Arab Emirates, 2019, pp. 11-80
- [18] Jefferson, W. T., *The Future of Geothermal Energy*, Technical Report., Massachusetts Institute of Technology, Cambridge, Mass., USA, 2007, pp. 1-372

## Appendix

Table 1. The equilibrium equations of related equipment for two power generation systems

Equipment	Single flash	Double flash	ORC	Flash-binary
Separator	$\dot{m}_1 = \dot{m}_3 + \dot{m}_6$ $\dot{m}_1 h_1 = \dot{m}_3 h_3 + \dot{m}_6 h_6$	$\dot{m}_1 = \dot{m}_3 + \dot{m}_7$ $\dot{m}_1 h_1 = \dot{m}_3 h_3 + \dot{m}_7 h_7$ $\dot{m}_7 = \dot{m}_9 + \dot{m}_{11}$ $\dot{m}_7 h_7 = \dot{m}_9 h_9 + \dot{m}_{11} h_{11}$	–	$\dot{m}_9 = \dot{m}_{11} + \dot{m}_{s1}$ $\dot{m}_9 h_9 = \dot{m}_{11} h_{11} + \dot{m}_{s1} h_{s1}$
Turbine for flash system	$\dot{m}_3 h_3 = \dot{m}_4 h_4 + W_{\text{flash}}$ $\eta_{\text{Turbine}} = (h_3 - h_4)/(h_3 - h_{4,s})$	$\dot{m}_3 h_3 = \dot{m}_4 h_4 + W_{\text{Turbine},1}$ $\eta_{\text{Turbine},1} = (h_3 - h_4)/(h_3 - h_{4,s})$ $\dot{m}_9 h_9 = \dot{m}_{10} h_{10} + W_{\text{Turbine},2}$ $\eta_{\text{Turbine},2} = (h_9 - h_{10})/(h_9 - h_{10,s})$	–	$\dot{m}_{11} h_{11} = \dot{m}_{12} h_{12} + W_{\text{flash}}$ $\eta_{\text{Turbine}} = (h_{11} - h_{12})/(h_{11} - h_{12,s})$
Condenser for flash system	$P_{\text{Con}} = P_5$ $\dot{m}_4(h_4 - h_5) = \dot{m}_{C1}(h_{C2} - h_{C1})$	$P_{\text{Con}} = P_5 = P_6$ $\dot{m}_5(h_5 - h_6) = \dot{m}_{C1}(h_{C2} - h_{C1})$	–	$P_{\text{Con}} = P_{13}$ $\dot{m}_{12}(h_{12} - h_{13}) = \dot{m}_{C4}(h_{C5} - h_{C4})$
Condenser for ORC	–	–	–	$P_{\text{Con}} = P_7 = P_8$ $\dot{m}_8(h_7 - h_8) = \dot{m}_{C2}(h_{C3} - h_{C2})$
Working pump	–	–	$W_{\text{pump}} = \dot{m}_1(h_1 - h_{10})$ $\eta_{\text{pump}} = (h_1 - h_{10})/(h_1 - h_{10,s})$	$W_{\text{pump}} = \dot{m}_8(h_1 - h_8)$ $\eta_{\text{pump}} = (h_1 - h_8)/(h_1 - h_{8,s})$
Recuperator for ORC	–	–	$\dot{m}_1(h_1 + h_7) = \dot{m}_8(h_2 + h_8)$	
Vaporizer for ORC	–	–	$\dot{m}_s = \dot{m}_{s1} = \dot{m}_{s4}$ $\dot{m}_1(h_6 - h_3) = \dot{m}_s(h_{s1} - h_{s4})$	$\dot{m}_2 = \dot{m}_3 = \dot{m}_4 = \dot{m}_5, \dot{m}_{k1} = \dot{m}_{k3}$ $\dot{m}_3(h_4 - h_3) = \dot{m}_{s2}(h_{s2} - h_{s3})$
Preheater for ORC	–	–	$\dot{m}_s = \dot{m}_{s4} = \dot{m}_{s5}$ $\dot{m}_1(h_3 - h_2) = \dot{m}_s(h_{s4} - h_{s5})$	$\dot{m}_1 = \dot{m}_2, \dot{m}_{s4} = \dot{m}_{s5}$ $\dot{m}_1(h_2 - h_1) = \dot{m}_{s4}(h_{s4} - h_{s5})$
Turbine for ORC	–	–	$\dot{m}_1 h_6 = \dot{m}_7 h_7 + W_{\text{binary}}$ $\eta_{\text{Turbine}} = (h_6 - h_7)/(h_6 - h_{7,s})$	$\dot{m}_3 h_5 = \dot{m}_6 h_6 + W_{\text{binary}}$ $\eta_{\text{Turbine}} = (h_5 - h_6)/(h_5 - h_{6,s})$

Table 2. Purchased equipment costs

Equipment	Cost [US\$]			
	Single flash	Double flash	ORC	Flash-binary
Separator	110451	143915	–	33864
Condenser	49409	59310	54067	69141
Turbine and generator	105193	153122	109797	124217
Vaporizer	–	–	35257	26285
Preheater	–	–	22678	10057
Recuperator	–	–	11540	–
Working fluid pump	–	–	7702	2866
Cooling water pump	7351	8824	13475	11165
Cooling tower	27316	34321	29133	34541
Purchased equipment costs	299719	399491	283649	312137

**Table 3. Total capital cost of surface and sub-surface system**

Item	Parameters	Cost, US\$			
		Single flash	Double flash	ORC	Flash-binary
Cost of sub-surface ( $C_{fuel, cost}$ )	Estimated by Wellcost Lite [18]	2200000	2200000	2200000	2200000
PEC ( $C_{PEC, cost}$ )	Estimated	299719	399491	283649	312137
Equipment installation cost	$33\% \times C_{PEC, cost}$	98907	131832	93604	103005
Pipeline cost	$35\% \times C_{PEC, cost}$	104902	139822	99277	109248
Instrument control cost	$12\% \times C_{PEC, cost}$	35966	47939	34038	37456
Electrical material cost	$13\% \times C_{PEC, cost}$	38964	51934	36874	40578
Civil engineer	$21\% \times C_{PEC, cost}$	62941	83893	59566	65549
Direct cost ( $C_{Direct, cost}$ )		2841399	3054911	2807008	2867973
Indirect cost	$15\% \times C_{Direct, cost}$	426210	458236	421051	430196
TCC ( $C_{Capital, cost}$ )		3267609	3513147	3228059	3298169